IEEE Access
Multidisciplinary | Rapid Review | Open Access Journal

Received March 1, 2019, accepted March 13, 2019, date of publication March 19, 2019, date of current version April 5, 2019.

*Digital Object Identifier 10.1109/ACCESS.2019.2906219*

# Active Frequency Selective Surface With Wide Reconfigurable Passband

**QINGXIN GUO[1], (Senior Member, IEEE), ZENGRUI LI[1], (Member, IEEE), JIANXUN SU[1], JIMING SONG[2], (Fellow, IEEE), AND LAMAR Y. YANG[3], (Senior Member, IEEE)**

[1]School of Information Engineering, Communication University of China, Beijing 100024, China
[2]Department of Electrical and Computer Engineering, Iowa State University, Ames, IA 50011, USA
[3]Department of Electrical and Computer Engineering, University of Nebraska–Lincoln, Lincoln, NE 68106, USA

Corresponding authors: Qingxin Guo (qxguo@cuc.edu.cn) and Zengrui Li (zrli@cuc.edu.cn)

This work was supported by the National Natural Science Foundation of China under Grant 61671415 and Grant 61331002.

**ABSTRACT** This paper presents an active frequency selective surface (AFSS) with a wide reconfigurable passband. The tuning mechanism was investigated with an equivalent circuit which consists of a parallel L–C resonant circuit and a series L–C resonant circuit. A cross-loop slot was selected as a unit cell, and varactor diodes were added across the slot to tune the passband. The effects of various bias configurations on the transmission coefficients were studied. The simulation results showed that a reconfigurable passband ranged from 2.92 to 5.74 GHz was obtained with a variable capacitance from 0.8 to 0.1 pF. A prototype of the proposed AFSS was fabricated and measured. The measurement results showed that the passband was altered from 2.94 to 5.66 GHz if the biasing voltage of varactor diodes was increased from 4 to 18V. The measurement and simulation results agree well with each other.

**INDEX TERMS** Tunable frequency selective surface (FSS), active frequency selective surface (AFSS), reconfigurable frequency selective surface (RFSS), varactor diode.

## I. INTRODUCTION

The frequency selective surface (FSS) has been extensively investigated in the past decades due to its widespread applications in the fields of antenna, absorber, radome and shielding [1]. With the rapid development of wireless technology, utilizations of the FSS for mitigating radio frequency (RF) interference or improvement of electromagnetic shielding are on the rise [2], [3]. The ability to electrically tune or alter the frequency response is in great demand for various applications. The frequency tuning characteristics of the FSS make it well suitable in applications for adaptive environments such as a tunable radome or adaptive shielding of unwanted wireless signals.

Several designs of reconfigurable FSS (RFSS) have been proposed in the literatures [4]–[6]. By using a magnetically tunable ferrite substrate, a RFSS has been developed in [4]. However, the design suffers from slow tuning speed and small tuning range. Some RFSSs have been designed based on liquid crystals [5]–[7], whose dielectric constant is altered by the bias voltage. But the tuning ranges of the liquid-crystal-based RFSS are relatively limited. Micro-electro-mechanical systems (MEMS)-based RFSSs are presented in [8]–[10]. Although MEMS devices are electrostatically actuated two-state switched capacitors which can provide continuous and smooth transitions between different operating status, this approach demands complicated fabrication methods. Moreover, these solid-state switches suffer from the nonlinearity and low isolation. Graphene-based RFSS has also been reported in recent years [11]–[13], but realizing such a structure is an enormous challenge due to the difficulty in controlling the surface conductivity.

Active components such as varactors [14]–[17] and PIN diodes [18]–[20] provide high-speed and wideband tuning with a compact size and low cost for tuning microwave devices. However, a DC voltage needs to be applied to the active component and RF/DC isolation should also be considered. Compared with designing a bias for RF circuits, it is more difficult for an FSS with active components. The main reason is that the bias wires and the active components consist of a new periodic structure which has to be added into the FSS. The interaction between two periodic structures exists inevitably, and hence the performances of original FSS are significantly affected. So far, most of RFSS with active

The associate editor coordinating the review of this manuscript and approving it for publication was Feng Lin.

components are presented for absorbers and bandstop filters, and very few bandpass RFSSs are proposed.

In this paper, an RFSS with a wide tunable passband is presented. A cross-loop slot was selected for the design. Because its equivalent circuit consists of a parallel $L$-$C$ resonant circuit and a series $L$-$C$ resonant circuit, both the transmission pole and zero can be tuned. Varactor diodes are utilized to realize the tuning of the passband. The effects of different bias configurations on the transmission coefficient under the oblique incidence were studied. The simulation results showed that a wide reconfigurable passband ranged from 2.92 to 5.74 GHz was realized. To verify the proposed design, the RFSS was fabricated and measured.

The remainder of this paper is organized as follows. Section II presents the circuit model and tuning principle of the presented RFSS. Section III describes different bias configurations and their effects. Section IV provides the fabrication and experimental verification. Finally, the conclusion is drawn in Section V.

## II. UNIT CELL DESIGN

It is well known that a parallel $L$-$C$ circuit acts as a band-pass filter and a series $L$-$C$ circuit acts as a band-stop filter. The resonant frequency of an $L$-$C$ circuit, either a parallel circuit or a series circuit, changes if $L$ and/or $C$ is altered. Practically speaking, tuning $C$ is cost-effective and easy to be achieved. During designing a reconfigurable filter, a consideration of using both parallel $L$-$C$ circuit and series $L$-$C$ circuit provides more degree-of-freedom, compared with only one parallel or series resonance circuit. Fig. 1(a) shows a filter with both a parallel $L$-$C$ resonant circuit and a series $L$-$C$ resonant circuit. The parallel $L_1$-$C_1$ provides a passband and the series $L_2$-$C_2$ provides a stopband or transmission zero. The ABCD matrix of the network can be written as

$$\begin{bmatrix} A & B \\ C & D \end{bmatrix} = \begin{bmatrix} 1 & 0 \\ \dfrac{1}{j\omega L_1} & 1 \end{bmatrix} \begin{bmatrix} 1 & 0 \\ j\omega C_1 & 1 \end{bmatrix} \begin{bmatrix} 1 & 0 \\ \dfrac{1}{j\omega L_2 + \dfrac{1}{j\omega C_2}} & 1 \end{bmatrix} = \begin{bmatrix} 1 & 0 \\ \dfrac{U_1 U_2 - \omega^2 L_1 C_2}{j\omega L_1 U_2} & 1 \end{bmatrix} \quad (1)$$

where $U_1 = 1 - \omega^2 L_1 C_1$ and $U_2 = 1 - \omega^2 L_2 C_2$.

Using the conversion formula between S matrix and ABCD matrix, $S_{11}$ and $S_{21}$ can be obtained [21] with

$$S_{11} = \frac{-Z_0 \left[U_1 U_2 - \omega^2 L_1 C_2\right]}{j2\omega L_1 U_2 + Z_0 \left[U_1 U_2 - \omega^2 L_1 C_2\right]} \quad (2)$$

$$S_{21} = \frac{j2\omega L_1 U_2}{j2\omega L_1 U_2 + Z_0 \left[U_1 U_2 - \omega^2 L_1 C_2\right]} \quad (3)$$

where $Z_0$ is the characteristic impedance of ports. If

$$\omega_2 = 1 \Big/ \sqrt{L_2 C_2} \quad (4)$$

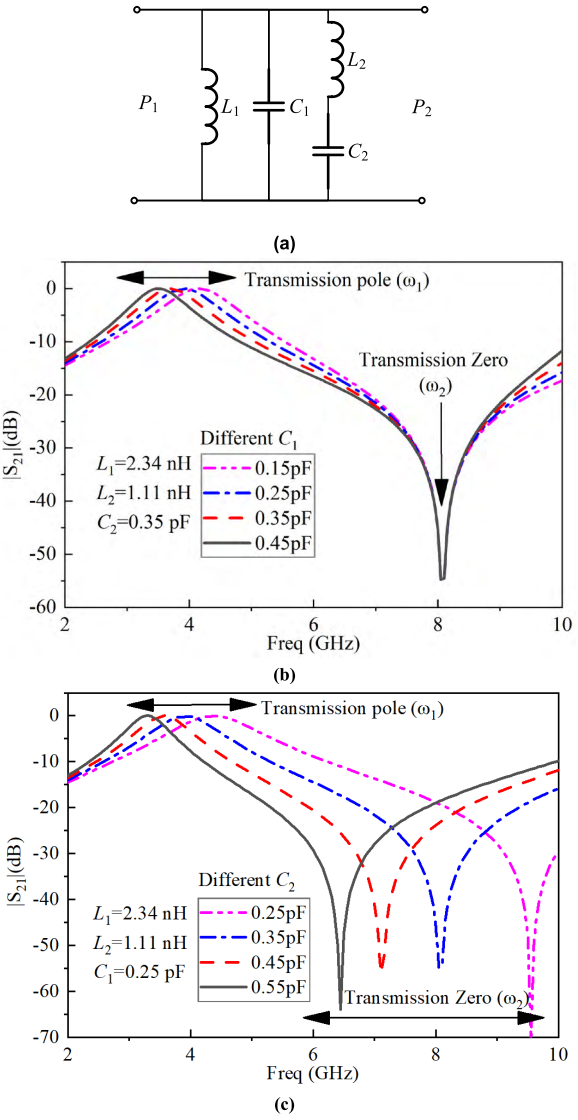


**FIGURE 1.** Lumped filter and responses. (a) Circuit. (b) Responses of different $C_1$. (c) Responses of different $C_2$.

then, $|S_{11}| = 1$ and $|S_{21}| = 0$, which means there is a transmission zero at $\omega_2$.

While at frequencies $\omega_1$ or $\omega_3$ given by

$$\omega_1^2 = \frac{U_3 - \sqrt{U_3^2 - 4L_1C_1L_2C_2}}{2L_1C_1L_2C_2} \quad (5)$$

$$\omega_3^2 = \frac{U_3 + \sqrt{U_3^2 - 4L_1C_1L_2C_2}}{2L_1C_1L_2C_2} \quad (6)$$

where $U_3 = L_1C_1 + L_2C_2 + L_1C_2$, $|S_{11}| = 0$ and $|S_{21}| = 1$ will be obtained. The result implies there are two transmission poles at $\omega_1$ and $\omega_3$.

From (2) - (5), we know that one passband around $\omega_1$ and one stopband around $\omega_2$ can be obtained. Altering $C_1$ changes the position of the transmission pole ($\omega_1$) but it cannot changes the transmission zero ($\omega_2$). However, altering

$C_2$ changes not only the position of the transmission pole but also the transmission zero. Fig. 1(b) and (c) show the frequency responses with different $C_1$ and $C_2$, respectively. The results were simulated with Ansys Electromagnetics Suite (Circuit Designer). It can be seen from Fig. 1(b) that the passband is altered but the transmission zero at about 8 GHz almost remain unchanged while only $C_1$ is changed. However, if $C_2$ increases, both the passband and the transmission zero decrease, as shown in Fig. 1(c). These results illustrate that the circuit shown in Fig. 1(a) has characteristics of both tunable passband and tunable stopband. In this paper, we concentrate on the passband tuning.

For an FSS with a bandpass characteristic, different types of slot elements have been presented [1]. Among those elements, the cross-loop slot element, which is also called as a four-legged loaded slot element, is often used. It is polarization independent due to the 90° -rotational symmetry structure. The electromagnetic behavior of the cross-loop slot that shown on the left of Fig. 2(a) can be approximately represented by the equivalent circuit model (ECM) shown in Fig. 1(a). The center frequency and the bandwidth of the passband are controlled not only by the inter-element spacing but also by the shape of the element, including the length, the gap and the width of the slot. The parameters of the ECM shown in Fig. 1(a) can be mapped to the geometrical dimensions of the FSS shown in Fig. 2(a) by using the method explained in [22]–[24].

In order to alter the passband of the FSS, we inserted four tunable capacitors ($VC_2$) across the slot in the diagonals, as shown on the right of Fig. 2(a). The FSS with different capacitances is simulated with Ansys electromagnetics suite (HFSS). The comparison results of the ECM and HFSS are shown in Fig. 2(b), and their corresponding parameters are listed in Table 1. It is evident that they agree very well with each other. It is worth to mention that the values of $C_1$ and $L_2$ differ slightly, and the dimensions ($W_1$, $W_2$, $W_3$ and $g_1$) of the FSS are invariant. The possible reasons include the dispersion of FSS or computational error. The differences between $VC_2$ and $C_2$ are always less than $0.08 \pm 0.01$ pF owing to the gap capacitance. The cell size $W_1$ is 12.5 mm, which is $\lambda_0/8$ at 3 GHz.

**TABLE 1. Parameters comparison.**

| Line | $L_1$ (nH) | $C_1$ (pF) | $L_2$ (nH) | $C_2$ (pF) | $VC_2$ (pF) | $f_p$ (GHz) | $f_s$ (GHz) |
|---|---|---|---|---|---|---|---|
| 1 | 2.045 | 0.225 | 1.420 | 0.180 | 0.1 | 5.14 | 9.9 |
| 2 | 2.045 | 0.240 | 1.371 | 0.275 | 0.2 | 4.44 | 8.18 |
| 3 | 2.045 | 0.242 | 1.359 | 0.375 | 0.3 | 3.96 | 7.06 |
| 4 | 2.045 | 0.243 | 1.331 | 0.580 | 0.5 | 3.32 | 5.94 |
| 5 | 2.045 | 0.255 | 1.311 | 0.889 | 0.8 | 2.75 | 4.65 |

| $W_1$ | $W_2$ | $W_3$ | $g_1$ |
|---|---|---|---|
| 12.5 mm | 12 mm | 2 mm | 0.5 mm |

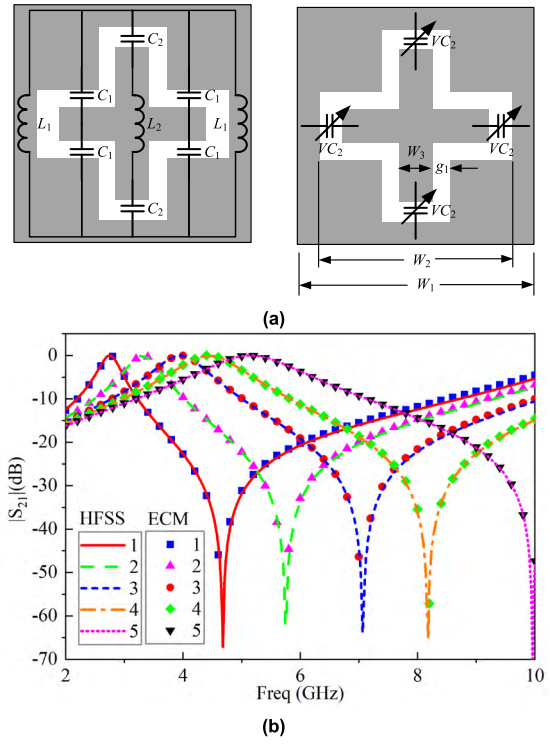


**FIGURE 2.** Unit cell and responses. (a) Configurations. (b) Comparison of $|S_{21}|$ from ECM and HFSS.

## III. DC BIAS NETWORK DESIGN

The varactor diode is often used in RF circuit design to tune the resonant frequency because its capacitance is inversely proportional to the square root of the applied voltage. A simplified equivalent circuit of the varactor diode is shown in Fig. 3 [25]. The parasitic inductance $L_s$ is associated with the package material, geometry and bonding wires or ribbons of the diode. The inductance $L_s$ is very small and can be ignored at low frequencies, but it is considered as constant at high frequencies. The series resistance, $R_s$, is a function of the applied voltage and operating frequency, and can also be considered constant too. The package capacitance $C_P$ is the fixed parasitic capacitance arising from the installation of the die in the package. The varactor junction capacitance $C_J$ is a function of the applied reverse DC voltage $V_R$. The relation between the junction capacitance $C_J$ and the reverse voltage $V_R$ is given by [25]

$$C_J = \frac{C_{J0}}{\left(1 + V_R/V_J\right)^M} \tag{7}$$

where $C_{J0}$ is the zero-bias junction capacitance, $V_J$ is the junction potential, $M$ is the grading coefficient. When increasing the reverse bias ($V_R$), the junction capacitance ($C_J$) decreases.

The tunable capacitors shown in Fig. 2 (a) can be realized by using the varactor diodes. For tuning the FSS, the varactors can provide high-speed and wideband tuning with a

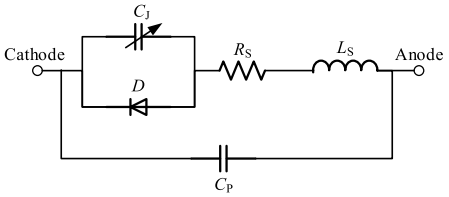


**FIGURE 3.** Equivalent circuit of a varactor diode [25].

compact size. However, a DC voltage needs to be applied as a reverse bias across each diode to alter its capacitance, and the RF/DC isolation also must be considered. We now describe how we add a DC bias network for the presented RFSS, and investigate the effects of different bias. As shown in Fig. 4(a), we placed four varactor diodes back to back in one element, that is to say, the cathode of each diode is connected with one leg of the inner cross and all anodes are connected to the outer conductor. One narrow strip is placed on the bottom layer and one via in the center of the cell connects the top layer and bottom layer. It is a quite neat structure, but the FSS exhibits polarization sensitivity, namely, the passbands are different for distrinct polarizations. Fig. 4(b) shows the transmission coefficient $|S_{21}|$ of different polarizations. The passband of TE polarization is increased significantly because an additional inductance $L_3$ is paralleled to $L_1$ (shown in Fig. 1(a)) and the total equivalent inductance is reduced after the DC bias is added.

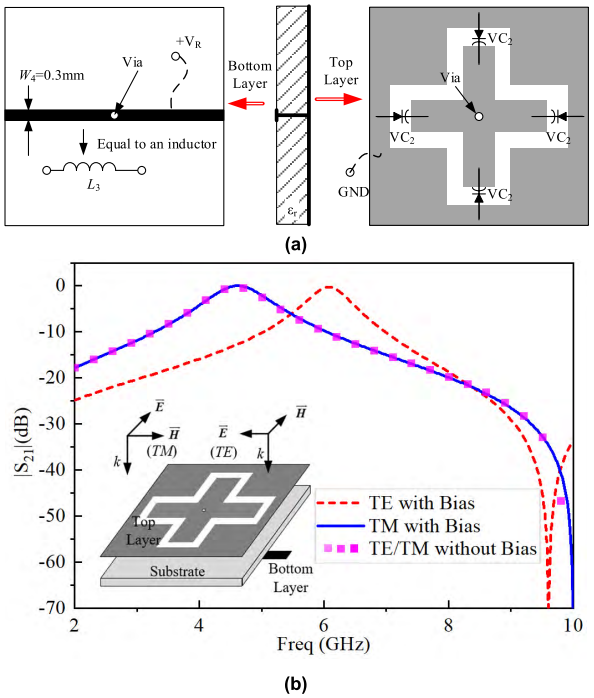


**FIGURE 4.** Structure and $|S_{21}|$ of DC bias with only one strip. (a) Structure. (b) $|S_{21}|$ of different polarizations.

To realize the polarization independence, a cross strip was used to replace the single strip, as shown in Fig. 5(a). Fig. 5(c) shows the $|S_{21}|$ of the oblique incidence on the $xz$ plane with an incident angle of 30°. It is observed from the figure that three singularities or transmission zeros emerge at 6.4, 8 and 9.8 GHz for the TM polarization, but no singularity appears for the TE polarization. Even worse, the singularity at 6.4 GHz happens to appear within the passband and the frequency response was significantly affected. Rotating the cross 45 degrees, as shown in Fig. 5(b), reduces the center frequency of the passband and makes the singularities out-of-band. Fig. 5(d) shows the simulation results. Comparing Fig. 5(c) and (d), it is seen that the passband is reduced from

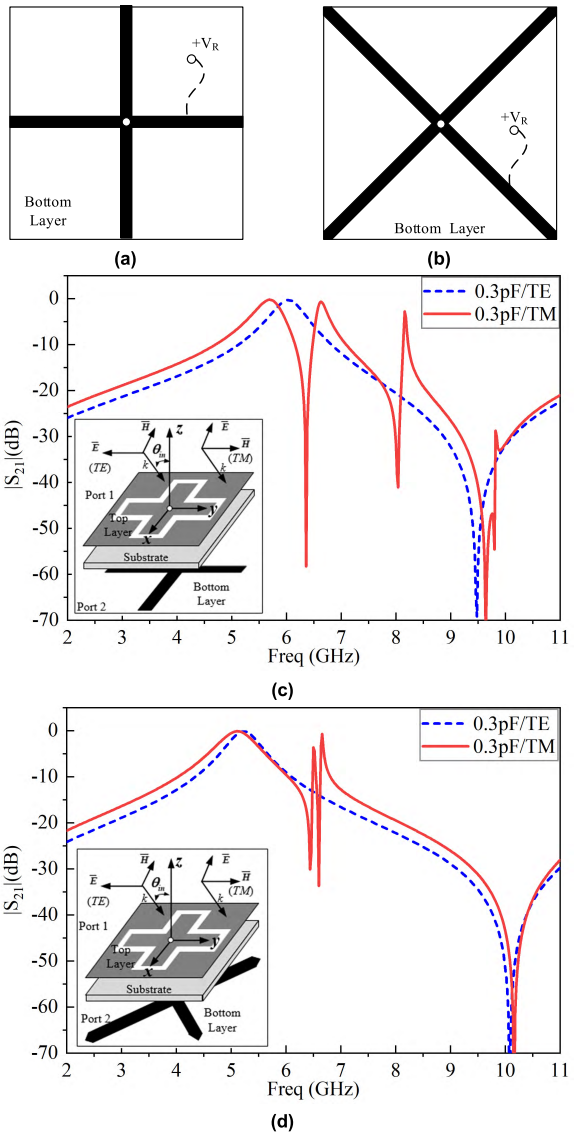


**FIGURE 5.** Different bias setups and the transmission coefficients under oblique incident of 30°. (a) Cross bias network. (b) Tilt-cross bias network. (c) $|S_{21}|$ of FSS with cross bias. (d) $|S_{21}|$ of FSS with tilt-cross bias.

around 6 GHz to near 4.8 GHz, and two singularities arise at around 6.4 and 6.6 GHz.

It is evident that these singularities only appear in the TM mode. Under oblique incidence, the electric field is parallel to the metallic surface for the TE mode, but tilt to the metallic surface for the TM mode. The tilted electric field of the TM mode induces two opposite currents flow along two close and opposite edges of the slot at 6.4 GHz, as shown in the left of Fig. 6(a). The electromagnetic fields produced by these two closed opposite currents do not radiate because they are cancelled with each other. The result means that the slot together with the varactor is resonant at 6.4 GHz. The current distribution of the TM mode at 8 GHz is shown in the left of Fig. 6(b). The currents on the top layer converge to the via and then flow along the biasing cross in the opposite direction. The via and two crosses form a resonant circuit at 8 GHz under the oblique incidence. Rotating the biasing

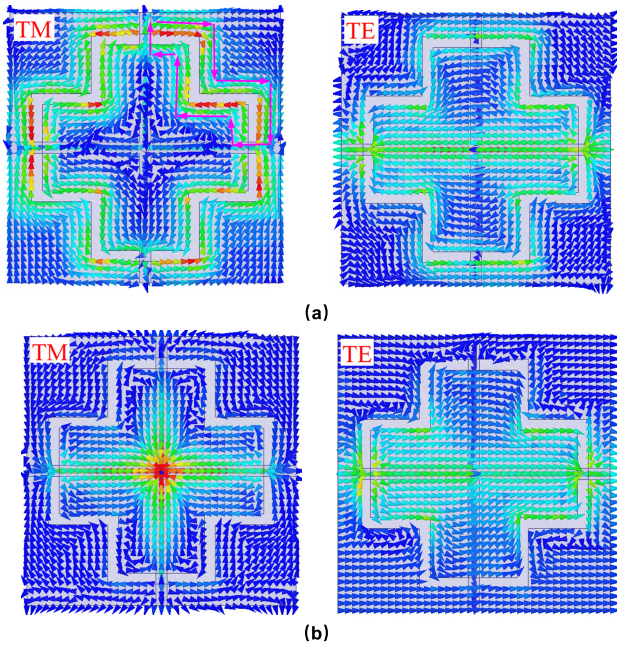


**FIGURE 6.** Current distributions under oblique incidence at 30°. (a) 6.4 GHz. (b) 8 GHz.

cross increases the equivalent inductance of the cross and decreases the resonance frequency from 8 to 6.6 GHz. The current distributions of the TE mode at 6.4 and 8 GHz are shown in the right of Fig. 6(a) and (b), respectively. The induced currents mainly flow along the axis of inner cross and radiate the electromagnetic power. Thus, the singularities only appear in the TM mode under the oblique incidence.

The next step is to remove the singularities excited by the tilt-cross, or at least to shift them far away from the passband. In designing RF circuits, the inductive chokes are often used for the suppression of electromagnetic interference (EMI) and radio frequency interference (RFI) from power supply lines and for prevention of malfunctioning of power electronics device. Lumped inductors are utilized in low frequency circuits, while distributed inductors such as meander lines and spiral inductors are often used in high frequency circuits. Unfortunately, both lumped inductors and distributed inductors are unsuitable for designing active filtering FSS. Firstly, the distributed inductor which is added to each element will produce another periodic structure and greatly affect the characteristics of the original FSS. Secondly, a lumped inductor always has a self-resonant frequency (SRF). Due to the parasitic effects of a lump inductor, the capacitive reactance dominates its impedance at the frequencies above the SRF.

Fortunately, the varactor diode operates in a reverse-biased state. Thus, a very low DC current flows through the device. Instead of using an inductor, a lumped or distributed resistor can be utilized for suppression of EMI. In the design, four lumped resistors of 20 kΩ were embedded into the tilt cross and placed just under the slot. Fig. 7(a) and (b) show the configuration and the simulation results of $|S_{21}|$, respectively. It is observed from Fig. 7(b) that only one singularity emerges at 6.4 GHz under 30° oblique incidence. The second singularity shown in Fig. 5 has been removed. It is worthwhile to mention that the frequency of the singularity is altered with the tuning of the varactors. The in-band insertion loss does not increase significantly after the resistors are added, owing to the resistors block the AC current flow along bias lines to the DC source.

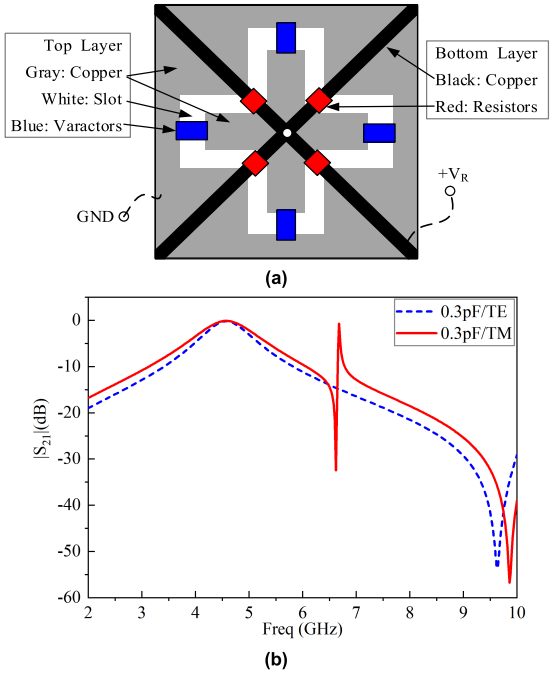


**FIGURE 7.** $|S_{21}|$ of RFSS fed by a tilt-cross with lumped resistors under the oblique incidence. (a) Configuration. (b) $|S_{21}|$.

## IV. RESULTS AND DISCUSSIONS

The proposed RFSS with a tunable passband was realized after the tunable unit cell of bandpass FSS and the DC bias network were properly designed. Simulation results of $|S_{21}|$ with different capacitances under the normal incidence are shown in Fig. 8. The center frequency of the passband decreases from 5.74 to 2.92 GHz with increasing of the capacitance from 0.1 to 0.8 pF.

To verify the design and simulation results discussed above, a prototype of the RFSS was fabricated using the standard printed circuit board (PCB) technology. The FSS was etched on the F4B substrate whose thickness and relative permittivity are 0.508 mm and 2.2, respectively. The overall size of the fabricated structure was 200 mm× 200 mm, in which there are 16 × 16 cells. The dimensions of $W_1$, $W_2$ and $W_3$ are 12.5, 10.5 and 2 mm, respectively. The photo of the prototype is shown in Fig. 9(a).

Practically, it is not easy to find a varactor diode which has nice feature of very low capacitance and high capacitance ratio. SMV2201-040LF from Skywork Solutions, Inc. was chosen for our experiment [25]. Its junction capacitance $C_J$ is changed from 0.24 to 0.8 pF if the reverse voltage $V_R$ decreases from 18 to 4 V. The model parameters shown in Fig. 3 are $C_p$ = 0.075 pF, $L_S$ = 0.45 nH, $R_S$ = 5.41Ω, respectively. The diodes in a cell were back-to-back

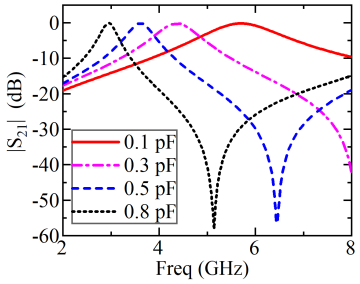


**FIGURE 8.** Simulation $|S_{21}|$ of RFSS.

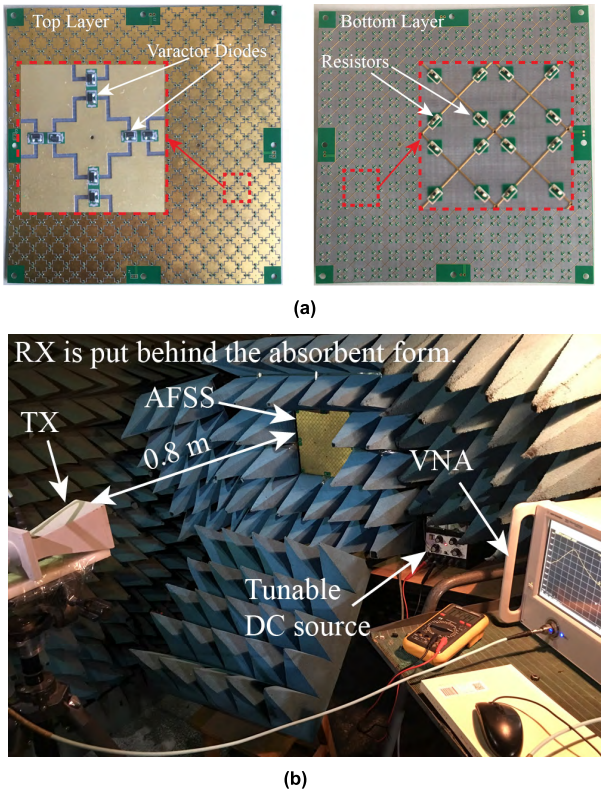


**FIGURE 9.** (a) Photo of the prototype. (b) Photo of the measurement setup.

soldered across the slot. The lumped resistors of 20 kΩ with 0402 package were used.

Figure 9(b) shows the measurement setup. The presented RFSS was measured in an anechoic chamber by using Keysight N5234A. In order to ensure the antenna was working at the far field range within testing band, the space between transmitting antenna (TX) or receiving antenna (RX) and the RFSS was 0.8 m. The aperture of two horn antennas for testing is 75 mm × 75 mm. The RFSS was surrounded with the commercial absorbent foam to reduce the effect of the edge diffraction.

Fig. 10 shows the comparison between the simulation and measurement results. Measured $|S_{21}|$ under three different reversed bias voltages, 4, 8 and 18V are shown in Fig. 10(a). The corresponding junction capacitors of varactor diodes are 0.8, 0.4 and 0.24 pF, which are given in the datasheet of the varactor diode. It is evident that the measured passband decreases from 4.66 to 2.92 GHz with the decreasing of the

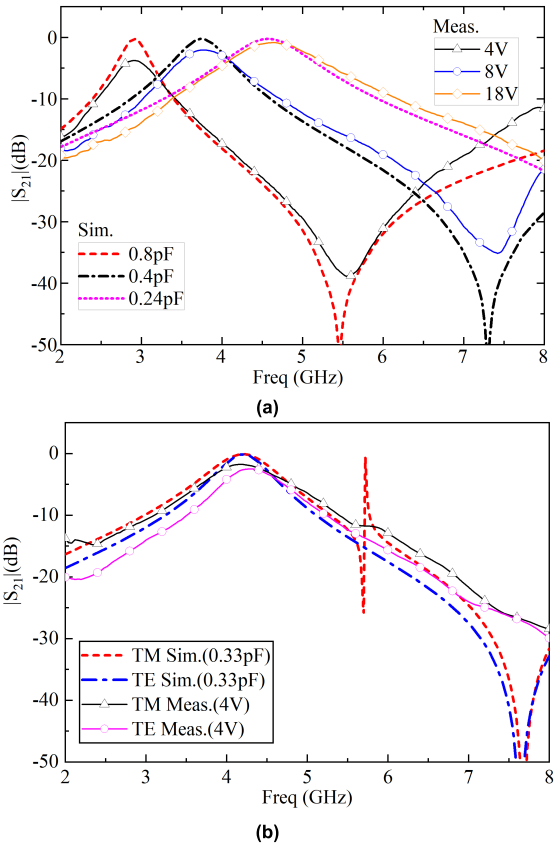


**FIGURE 10.** (a) $|S_{21}|$ measured under different reversed voltages and simulated with different capacitances. (b) results of the oblique incidence at 30°.

reversed voltage from 18 to 4 V. Fig. 10(b) shows the results under the oblique incidence at 30°. Some discrepancies exist between the simulation and measurement results. All measurement insertion losses are a little bit larger than that of the simulation results, especially at the low frequencies where the varactors were operated under the low bias voltages. In the measured TM curve, a small ripple appears around the singularity which is shown in the simulated TM result. The main reason for these deviations might be the truncation of the structure, because an infinite periodic array was simulated by using one cell and Floquet ports in HFSS, but only a finite array has been fabricated and measured. Another reason might be because some distribution parameters such as the package and soldered dot of the varactor diodes were not taken into account during the simulations.

**TABLE 2.** A comparison between this work and some existing works.

| REF | Tunable range (GHz) | Insertion loss (dB) | Cell size @ the lowest frequency |
|---|---|---|---|
| [15] | 2.2-3.1 (34%) | <4 | 16mm (λ/8.5) |
| [16] | 3.7-5.2 (34%) | 6-3 | 8mm (λ/10.1) |
| [17] | 3.4-5.1 (40%) Sim. | 5-0.4 | 10.2mm (λ/8.6) |
| This work | 2.92-4.66 (46%) | 4.5-1 | 12.5mm (λ/8.2) |

A comparison between the designed tunable FSS and some existing tunable FSSs with some tuning mechanism is provided in Table 2 in terms of the tuning range and insertion

loss. The table shows that the proposed FSS improved the tuning range up to 46%.

## V. CONCLUSION

An RFSS with a wide reconfigurable passband is presented in this paper. The unit cell was designed with a cross-loop slot, which has an equivalent circuit consisting of both parallel and series resonances. The passband and stopband of the RFSS are tuned by using varactor diodes. The DC bias network which is indispensable for varactor diodes significantly affects the transmission coefficient of the RFSS. Three different configurations were investigated. Adding lumped resistors into the bias lines can mitigates the singularity excited by the bias network. The simulation results show that the passband of the RFSS decreases from 5.74 to 2.92 GHz with increasing of the capacitance from 0.1 to 0.8 pF, under the conditions of most model parameters of the varactor diodes were considered. The presented RFSS has been fabricated and measured. The measured passband is decreased from 4.66 to 2.92 GHz with the decreasing of the reversed voltage from 18 to 4 V.

## REFERENCES

[1] B. A. Munk, *Frequency Selective Surfaces: Theory and Design*. New York, NY, USA: Wiley, 2000.
[2] S. Celozzi, R. Araneo, and G. Lovat, *Electromagnetic Shielding*, 1st ed. New York, NY, USA: Wiley, 2008.
[3] D. Li, T.-W. Li, E.-P. Li, and Y.-J. Zhang, "A 2.5-D angularly stable frequency selective surface using via-based structure for 5G EMI shielding," *IEEE Trans. Electromagn. Compat.*, vol. 60, no. 3, pp. 768–775, Jun. 2018.
[4] T. K. Chang, R. J. Langley, and E. A. Parker, "Frequency selective surfaces on biased ferrite substrates," *Electron. Lett.*, vol. 30, no. 15, pp. 1193–1194, Jul. 1994.
[5] G. Yang, W. Kong, M. Chang, X. Liu, and Q. Wu, "Wideband tuning range frequency selective surface based on liquid crystal and tunable ability analysis," in *Proc. IEEE Conf. Electromagn. Field Comput. (CEFC)*, Miami, FL, USA, Nov. 2016, p. 1. doi: 10.1109/CEFC.2016.7816174.
[6] J. A. Bossard *et al.*, "Tunable frequency selective surfaces and negative-zero-positive index metamaterials based on liquid crystals," *IEEE Trans. Antennas Propag.*, vol. 56, no. 5, pp. 1308–1320, May 2008.
[7] W. Hu *et al.*, "Liquid crystal tunable mm wave frequency selective surface," *IEEE Microw. Wireless Compon. Lett.*, vol. 17, no. 9, pp. 667–700, Sep. 2007.
[8] M. Safari, C. Shafai, and L. Shafai, "X-band tunable frequency selective surface using MEMS capacitive loads," *IEEE Trans. Antennas Propag.*, vol. 63, no. 3, pp. 1014–1021, Mar. 2015.
[9] G. M. Coutts, R. R. Mansour, and S. K. Chaudhuri, "Microelectromechanical systems tunable frequency-selective surfaces and electromagnetic-bandgap structures on rigid-flex substrates," *IEEE Trans. Microw. Theory Techn.*, vol. 56, no. 7, pp. 1737–1746, Jul. 2008.
[10] B. Schoenlinner, A. Abbaspour-Tamijani, L. C. Kempel, and G. M. Rebeiz, "Switchable low-loss RF MEMS Ka-band frequency-selective surface," *IEEE Trans. Microw. Theory Techn.*, vol. 52, no. 11, pp. 2474–2481, Nov. 2004.
[11] X. Li, L. Lin, L.-S. Wu, W.-Y. Yin, and J.-F. Mao, "A bandpass graphene frequency selective surface with tunable polarization rotation for THz applications," *IEEE Trans. Antennas Propag.*, vol. 65, no. 2, pp. 662–672, Feb. 2017.
[12] D.-W. Wang *et al.*, "Tunable THz multiband frequency-selective surface based on hybrid metal–graphene structures," *IEEE Trans. Nanotechnol.*, vol. 16, no. 6, pp. 1132–1137, Nov. 2017.
[13] M.-L. Zhai and D.-M. Li, "Tunable hybrid metal–graphene frequency selective surfaces based on split-ring resonators by leapfrog ADI-FDTD method," *Micro Nano Lett.*, vol. 13, no. 9, pp. 1276–1279, Sep. 2018.
[14] S. Ghosh and K. V. Srivastava, "Broadband polarization-insensitive tunable frequency selective surface for wideband shielding," *IEEE Trans. Electromagn. Compat.*, vol. 60, no. 1, pp. 166–172, Feb. 2018.
[15] D. Ferreira, R. F. da Silva Caldeirinha, I. Cuiñas, and T. R. Fernandes, "Tunable square slot FSS EC modelling and optimisation," *IET Microw., Antennas Propag.*, vol. 11, no. 5, pp. 737–742, Apr. 2017.
[16] A. Ebrahimi, Z. Shen, W. Withayachumnankul, S. F. Al-Sarawi, and D. Abbott, "Varactor-tunable second-order bandpass frequency-selective surface with embedded bias network," *IEEE Trans. Antennas Propag.*, vol. 64, no. 5, pp. 1672–1680, May 2016.
[17] A. Ebrahimi, W. Withayachumnankul, S. F. Al-Sarawi, and D. Abbott, "Higher-order tunable frequency selective surface with miniaturized elements," in *Proc. IEEE 15th Medit. Microw. Symp. (MMS)*, Lecce, Italy, Nov./Dec. 2015, pp. 1–4.
[18] D. F. Mamedes, A. G. Neto, J. C. E Silva, and J. Bornemann, "Design of reconfigurable frequency-selective surfaces including the PIN diode threshold region," *IET Microw., Antennas Propag.*, vol. 12, no. 9, pp. 1483–1486, Jul. 2018.
[19] H. Li, Q. Cao, L. Liu, and Y. Wang, "An improved multifunctional active frequency selective surface," *IEEE Trans. Antennas Propag.*, vol. 66, no. 4, pp. 1854–1862, Apr. 2018.
[20] H. Fabian-Gongora, A. E. Martynyuk, J. Rodriguez-Cuevas, and J. I. Martinez-Lopez, "Active dual-band frequency selective surfaces with close band spacing based on switchable ring slots," *IEEE Microw. Wireless Compon. Lett.*, vol. 25, no. 9, pp. 606–608, Sep. 2015.
[21] D. M. Pozar, *Microwave Engineering*. Hoboken, NJ, USA: Wiley, 2009.
[22] D. Ferreira, R. Caldeirinha, I. Cuiñas, and T. Fernandes, "Square loop and slot frequency selective surfaces study for equivalent circuit model optimization," *IEEE Trans. Antennas Propag.*, vol. 63, no. 9, pp. 3947–3955, Sep. 2015.
[23] N. Behdad and M. A. Al-Joumayly, "A generalized synthesis procedure for low-profile, frequency selective surfaces with odd-order bandpass responses," *IEEE Trans. Antennas Propag.*, vol. 58, no. 7, pp. 2460–2464, Jul. 2010.
[24] O. Luukkonen *et al.*, "Simple and accurate analytical model of planar grids and high-impedance surfaces comprising metal strips or patches," *IEEE Trans. Antennas Propag.*, vol. 56, no. 6, pp. 1624–1632, Jun. 2008.
[25] *SMV2201 Varactors Datasheet*. Accessed: 2019. [Online]. Available: http://www.skyworksinc.com

**QINGXIN GUO** (SM'12) received the B.S., M.S., and Ph.D. degrees in electromagnetic field and microwave technology from the Communication University of China, Beijing, China, in 1997, 2006, and 2013, respectively.

From 1997 to 2002, he was an Engineer of Xiamen Overseas Chinese Electronics Co., Ltd., where he was involved with the repeaters and the mobile phone for the GSM system. From 2002 to 2004, he was a Project Manager of Beijing Gigamega Electronics Co., Ltd., where he was responsible for the design of amplifier for transmitter. From 2004 to 2008, he was an Engineer and a Project Manager of Beijing Filcom Technology Co. Ltd., where he was responsible for the design of combiner and multiplexer. In 2006, he joined the Communication University of China, where he has been an Associate Professor with School of Information Engineering, since 2013. From 2011 to 2012, he was a Visiting Researcher with the Electromagnetic Communication Laboratory, Electrical Engineering Department, Pennsylvania State University. His research interests include the antennas, microwave passive components, RF circuits, and metamaterial.

**ZENGRUI LI** received the B.S. degree in communication and information system from Beijing Jiaotong University, Beijing, China, in 1984, the M.S. degree in electrical engineering from the Beijing Broadcasting Institute, Beijing, in 1987, and the Ph.D. degree in electrical engineering from Beijing Jiaotong University, Beijing, in 2009. He has studied in Yokohama National University, Japan, from 2004 to 2005.

He is currently a Professor with the Communication University of China, Beijing. His research interests include computational electromagnetics, the finite-difference time-domain methods, electromagnetic modeling and simulation of antennas, and communication antennas. He is a Senior Member of the Chinese Institute of Electronics.

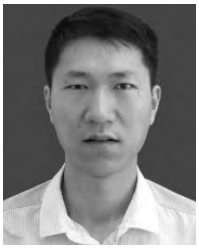

**JIANXUN SU** received the B.S. degree in electronic information engineering from the Taiyuan University of Technology, Taiyuan, China, in 2006 the M.S. degree in electromagnetic field and micro-wave technology from the Communication University of China, Beijing, China, in 2008, and the Ph.D. degree in electromagnetic field and micro-wave technology from the Beijing Institute of Technology, Beijing, in 2011.

From 2012 to 2014, he was with China Electronics Technology Group Corporation, where he engaged in phased-array system research. He is currently an Associate Researcher with the School of Information Engineering, Communication University of China, and also with the Science and Technology on Electromagnetic Scattering Laboratory. His current research interests include integral equation method, metamaterial, phased-array antenna, and radar target characteristics.

**JIMING SONG** (S'92–M'95–SM'99–F'14) received the B.S. and M.S. degrees in physics from Nanjing University, Nanjing, China, in 1983 and 1988, respectively, and the Ph.D. degree in electrical engineering from Michigan State University, East Lansing, MI, USA, in 1993.

From 1993 to 2000, he was a Postdoctoral Research Associate, a Research Scientist, and a Visiting Assistant Professor with the University of Illinois at Urbana–Champaign, Champaign, IL, USA. From 1996 to 2000, he was a part time Research Scientist with SAIC-Champaign, (formerly Demaco, Inc.), Champaign. He was a Principal Staff Engineer/Scientist with Semiconductor Products Sector of Motorola, Tempe, AZ, USA. In 2002, he joined the Department of Electrical and Computer Engineering, Iowa State University, Ames, IA, USA, as an Assistant Professor, where he is currently a Professor. He is also a Visiting Professor with the School of Information Engineering, Communication University of China, Beijing, China. He has authored the IEEE FAST ILLINOIS SOLVER CODE. His current research interests include the modeling and simulations of interconnects on lossy silicon and RF components, electromagnetic wave scattering using fast algorithms, the wave propagation in metamaterials, acoustic and elastic wave propagation and nondestructive evaluation, and transient electromagnetic field.

Dr. Song is an ACES Fellow. He was selected as a National Research Council/Air Force Summer Faculty Fellow in 2004 and 2005. He was a recipient of the NSF Career Award in 2006. He is an Associate Editor of IEEE ANTENNAS AND WIRELESS PROPAGATION LETTERS and *ACES Express*.

**LAMAR Y. YANG** (S'02–M'09–SM'09) received the B.S. degree in electrical engineering from Northern Jiaotong University, China, the M.S. degree in electrical engineering from the Beijing Broadcast Institute, China, and the Ph.D. degree in wireless communications and networks from The University of Texas at Austin, in 2006. He is currently an Associate Professor with the Department of Computer and Electronics Engineering, University of Nebraska–Lincoln. His current research interests include wireless communications and networks with emphasis on radio channel characterizations, cognitive radio networks, and statistical signal processing.

Dr. Yang has served as a Technical Program Committee Member for many years for numerous top ranked conferences, such as GLOBECOM, ICC, VTC, WCNC, and MSWiM. He served as a Reviewer for the IEEE TRANSACTIONS ON WIRELESS COMMUNICATIONS, the IEEE TRANSACTIONS ON VEHICULAR TECHNOLOGY, the IEEE TRANSACTIONS ON CIRCUITS AND SYSTEMS FOR VIDEO TECHNOLOGY, and the IEEE COMMUNICATIONS LETTERS.